Experimental Investigation of the Breakdown of the Onsager-Casimir Relations

C. A. Marlow,[1,*] R. P. Taylor,[1] M. Fairbanks,[1] I. Shorubalko,[2] and H. Linke[1,†]

[1]*Materials Science Institute, Physics Department, University of Oregon, Eugene Oregon 97403-1274, USA*

[2]*Institute of Solid State Physics, University of Latvia, Kengarga 8, LV-1063, Riga, Latvia*

(Received 12 October 2005; published 20 March 2006)

We use magnetoconductance fluctuation measurements of phase-coherent semiconductor billiards to quantify the contributions to the nonlinear electric conductance that are asymmetric under reversal of magnetic field. We find that the average asymmetric contribution is linear in magnetic field (for magnetic flux much larger than 1 flux quantum) and that its magnitude depends on billiard geometry. In addition, we find an unexpected asymmetry in the power spectrum of the magnetoconductance with respect to reversal of magnetic field and bias voltage.

DOI: 10.1103/PhysRevLett.96.116801 PACS numbers: 73.23.−b, 73.50.Fq, 75.47.Jn

Symmetry relations between transport coefficients are widely used to simplify calculations and to test the reliability of experiments. Understanding the physical mechanisms that leads to the breakdown of such relations is therefore both of practical and fundamental interest. Electron transport in linear response is characterized by a high degree of symmetry with respect to the direction of an applied magnetic field, B, as described by the Onsager-Casimir relations $\sigma_{\alpha\beta}(B) = \sigma_{\beta\alpha}(-B)$ in terms of the local conductivity tensor [1]. For the case of two-terminal mesoscopic conductors, this corresponds to the reciprocity theorem, which predicts the conductance is an even function of B in linear response [2]. At zero magnetic field, it is well-known that the absence of spatial symmetry leads to nonlinear terms in the conductance that are asymmetric with respect to bias voltage, V [3]. Only very recently has a distinct nonlinear term attracted attention that leads to an asymmetry of the conductance in the presence of both finite B and V [4,5]. The contribution of electron-electron interaction to this asymmetry was calculated for disordered [6] and ballistic [7] phase-coherent conductors for a magnetic flux smaller than 1 flux quantum $\Phi_0 = h/e$, and for V smaller than the characteristic energy scale of the system (typically μeV in semiconductor billiards).

Here we quantitatively investigate conductance asymmetries in a new regime, namely, for magnetic fields B much greater than one flux quantum threaded through the device area A, and for significant V (on order of mV) using billiards of varying geometry. Using measurements of magnetoconductance fluctuations (MCFs) we quantify, for the first time, the lowest nonlinear conductance term that leads to the breakdown of the Onsager-Casimir relations in this regime, and show that its magnitude is related to billiard geometry. We have also discovered that in addition to the individual features of the MCF, unexpectedly, the characteristics of the MCF power spectrum are asymmetric in B and V, and depend on device asymmetry.

The nonlinear differential conductance, $g(B, V) = dI/dV$, can be approximated by an expansion in V,

$$g(B, V) \equiv \frac{dI(B, V)}{dV} = g_0(B) + g_1(B)V + g_2(B)V^2 + g_3(B)V^3 \ldots \quad (1)$$

where $g_0(B)$ is the conductance in linear response. Each coefficient, $g_i(B)$, is the sum of an odd, $g_i^{\text{odd}}(B)$, and an even, $g_i^{\text{even}}(B)$, function of B. The odd contributions to the nonlinear conductance can be isolated by computing the value $\delta^{\text{odd}} \equiv g(+B, +V) - g(-B, +V) - g(+B, -V) + g(-B, -V)$ in combination with Eq. (1) [8], which to leading order in V gives

$$\delta^{\text{odd}} = 2\sum_{i=\text{odd}} [g_i(+B) - g_i(-B)]V^i = 4g_1^{\text{odd}}(B)V + \cdots. \quad (2)$$

In a similar way, the even contributions can be isolated by the sum $\delta^{\text{even}} \equiv g(+B, +V) + g(-B, +V) - g(+B, -V) - g(-B, -V)$, which when combined with Eq. (1) is

$$\delta^{\text{even}} = 2\sum_{i=\text{odd}} [g_i(+B) - g_i(-B)]V^i = 4g_1^{\text{even}}(B)V + \cdots. \quad (3)$$

Equations (2) and (3) can then be used to extract the odd and even components of $g_1(B)$ in Eq. (1) from the experimental data.

Conductance measurements were made on two-terminal semiconductor billiards defined using electron beam lithography and deep wet etching of the two-dimensional electron gas (2DEG) formed in a GaInAs/InP heterostructure (Fermi energy = 35 meV) [9]. This system was chosen for its high shape fidelity in billiard definition [5,9] and because previous studies have shown it exhibits negligible circuit-induced asymmetry, permitting careful control of device and conductance symmetry [4,5]. Device dimensions were smaller than the electron mean free path such that transport within the billiard was ballistic (see Table I). Device geometries were designed to have either

 © 2006 The American Physical Society

TABLE I. Experimental details for all devices used in this study: billiard area, A determined from depletion measurements, the electron mean free path, l_μ determined from electron mobility measurements, the phase-breaking length, l_ϕ at $T = 240$ mK for $V = 0$ and $V = 1$ mV determined using a correlation field analysis [10], the average rms of the fluctuations in linear response, linear-response conductance $\langle g_0^{\text{even}} \rangle$, the noise level $\langle g_0^{\text{odd}} \rangle$, and the calculated nonlinear coefficients $\langle g_1^{\text{odd}} \rangle$ and $\langle g_1^{\text{even}} \rangle$.

Device (asymmetry)	Area (μm^2)	l_μ (μm)	l_ϕ (μm) $V = 0$	l_ϕ (μm) $V \approx 1$ mV	Av rms $V = 0$ (e^2/h)	$\langle g_0^{\text{even}} \rangle$ (e^2/h) $V = 0$	$\langle g_0^{\text{odd}} \rangle$ (e^2/h)	$\langle g_1^{\text{odd}} \rangle$ (e^2/h)/mV · T	$\langle g_1^{\text{even}} \rangle$ (e^2/h)/mV
A (-)	0.72	6.2	19	13	0.1	5.3	0.012	0.008	0.013
B (LR)	0.49	6.1	13	11	0.1	5.6	0.012	0.015	0.035
C (UD)	0.5	6.1	16	15	0.1	10	0.014	0.044	0.016
D (UD)	3.5	4	25	24	0.04	3.3	0.01	0.026	0.011

left-right (LR) or up-down (UD) asymmetry. In the case of LR asymmetry, device symmetry is broken in the direction parallel to the current flow [device B in Fig. 1(c)] and the device potential is asymmetric under reversal of V. For UD asymmetry, symmetry is broken in the direction perpendicular to the current flow [devices C and D in Figs. 1(d) and 1(e)] and the potential is asymmetric with reversal of B. Device A [Fig. 1(b)] was included as a control since it nominally contains neither LR nor UD asymmetry. Measurements were made with a B field applied perpendicular to the 2DEG at a temperature $T = 240$ mK with several propagating channels. Transport was phase coherent (see Table I), leading to MCFs arising from quantum interference effects. MCFs are an excellent tool for probing transport symmetries in the nonlinear regime [5] since they are extremely sensitive to electron scattering configurations [11] and have a high degree of reproducibility. Two-terminal magnetoconductance measurements were made in four-point geometry using lock-in techniques. A tunable dc bias, V, was added to a small ac signal ($V_{\text{ac}} < kT/e \approx 20\ \mu$V) and measurements were taken for the various billiard geometries for both directions of B at several $\pm V$ and over the range of $B = 0$ to 0.5 T extending to $B \gg \Phi_0/A$. Voltages were chosen such that $eV \gg E_s$, where E_s is the mean energy level spacing in the billiard.

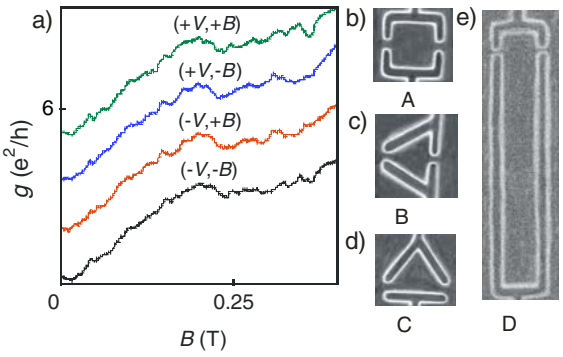

FIG. 1 (color online). (a) Magnetoconductance fluctuations measured on device C with an applied bias $|V| = 1.44$ mV for all four combinations of the sign of V and direction of B. MCFs are offset for clarity. (b), (c), (d), (e) scanning electron microscopy images of all devices used in this study.

First, we determine the functional dependence of the asymmetric nonlinear contributions on B. Figure 1(a) shows MCF measured in the four different configurations of $\pm V$ and $\pm B$ for device C at $V = 1.44$ mV. The MCF data are summed according to Eqs. (2) and (3) to determine δ^{odd} and δ^{even}, respectively, as a function of B. In Fig. 2(a), we plot $(\delta^{\text{odd}})^2$ and observe an overall increase with B, whereas the even part, $(\delta^{\text{even}})^2$, on average does not change significantly with B [Fig. 2(d)]. Because of their origin in MCF, δ^{odd} and δ^{even} fluctuate with B on the scale of the correlation field $B_c \approx \Phi_0/A \sim 4$ mT [11]. In order to compare the magnitude of δ^{odd} and δ^{even} it is necessary to perform averaging over a range of B values. We calculate $\langle \delta^{\text{odd}}(B_0) \rangle$, defined as the rms of δ^{odd} (B) within a window $[B_0 - \Delta B/2;\ B_0 + \Delta B/2]$ centered at B_0 where $\Delta B = 0.17\ \text{T} \sim 40 B_c$.

We find that $\langle \delta^{\text{odd}}(B_0) \rangle$ increases linearly as a function of V [see Fig. 2(b)], consistent with Eq. (1), confirming that

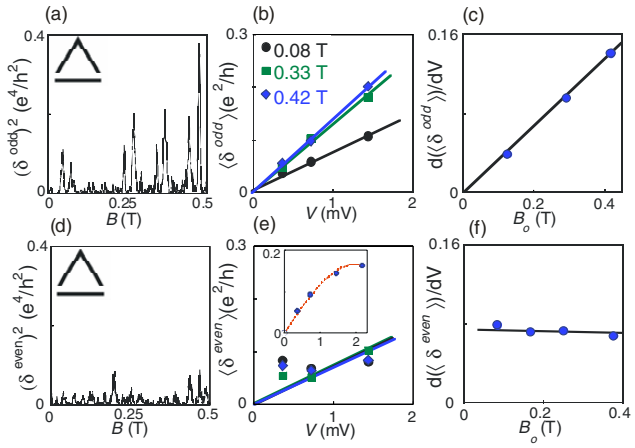

FIG. 2 (color online). Asymmetry analysis of MCFs for device C. (a) $(\delta^{\text{odd}})^2$ as a function of B, (b) $\langle \delta^{\text{odd}}(B_0) \rangle$ as a function of V. For clarity only select B_0 values are shown. (c) Slopes $d\langle \delta^{\text{odd}}(B_0) \rangle / dV$ of the linear fits in (b) as a function B_0, (d) $(\delta^{\text{even}})^2$ as a function of B, (e) $\langle \delta^{\text{even}}(B_0) \rangle$ as a function of V, for the same B_0 values shown in (b). (f) the slope $d\langle \delta^{\text{even}}(B_0) \rangle / dV$, determined from (e), with B_0. Linear fits in (b), (c), and (e) are forced through zero consistent with the definition of δ^{odd} and δ^{even} in Eqs. (2) and (3). The inset in (f) shows $\langle \delta^{\text{even}} \rangle$ with V, this time averaging data for all B_0, along with a fit of the form $c_1 V + c_3 V^3$.

the expansion holds for the dc-bias range used. The rms value of $g_1^{\mathrm{odd}}(B)$, $\langle g_1^{\mathrm{odd}}(B)\rangle$, can be determined by plotting the slopes, $d[\langle\delta^{\mathrm{odd}}(B_0)\rangle]/dV$, of the linear fits in Fig. 2(b) as a function of B_0 [Fig. 2(c)]. A linear dependence of $d[\langle\delta^{\mathrm{odd}}(B_0)\rangle]/dV$ with B_0 is observed, indicating $\langle g_1^{\mathrm{odd}}(B)\rangle$ is of the form $\langle g_1^{\mathrm{odd}}(B)\rangle = \langle g_1^{\mathrm{odd}}\rangle B$, where $\langle g_1^{\mathrm{odd}}\rangle$ is a constant determined from the slope in Fig. 2(c). As we show in Figs. 2(e) and 2(f) the even contribution $\langle\delta^{\mathrm{even}}(B_0)\rangle$ notably does not vary with B_0, indicating that $\langle g_1^{\mathrm{even}}(B)\rangle$ is of the form $\langle g_1^{\mathrm{even}}(B)\rangle = \langle g_1^{\mathrm{even}}\rangle$. Using this independence of B_0, we replot $\langle\delta^{\mathrm{even}}\rangle$ in the inset of Fig. 2(e), this time averaging data for all B_0, and find that $\langle\delta^{\mathrm{even}}\rangle$ depends on V as $c_1V + c_3V^3$, consistent with the expansion in Eq. (1). As the first key result of this Letter, we therefore conclude that the functional dependence of the nonlinear conductance has the form

$$\langle g(B, V)\rangle = \langle g_0^{\mathrm{even}}(B)\rangle + \langle g_1^{\mathrm{even}}\rangle V + \langle g_1^{\mathrm{odd}}\rangle BV \quad (4)$$

where $\langle g_0^{\mathrm{even}}(B)\rangle$ is the average magnetoconductance in linear response and the coefficients $\langle g_1^{\mathrm{odd}}(B)\rangle$ and $\langle g_1^{\mathrm{even}}(B)\rangle$ can be found through the analysis shown in Fig. 2. The term $\langle g_0^{\mathrm{odd}}(B)\rangle$ is not included in Eq. (4) because reciprocity requires $g_0^{\mathrm{odd}}(B) = 0$, consistent with the fact that the measured $\langle g_0^{\mathrm{odd}}(B)\rangle \approx 0.012e^2/h$ is comparable to the noise in our measurements determined by measuring the rms of the difference between MCF measured days apart in nominally identical configuration. Equation (4) is an empirical result which describes the behavior of the nonlinear conductance for $B \gg \Phi_0/A$ and $V \gg E_s/e$. Having established this basic form, it is now possible to investigate the role of device asymmetry in the nonlinear contributions in Eq. (4). The constants $\langle g_1^{\mathrm{even}}\rangle$ and $\langle g_1^{\mathrm{odd}}\rangle$ were determined for all billiards shown in Table I, along with the experimentally measured value $\langle g_0^{\mathrm{odd}}\rangle$ shown as a baseline for experimental noise. Significantly, devices C and D, which are both UD asymmetric, have significantly larger $\langle g_1^{\mathrm{odd}}\rangle$ values than devices A and B which lack UD asymmetry. This result is consistent with basic symmetry arguments [4,5]; in the case of UD asymmetry, electrons directed by the magnetic field to the top of the billiard encounter a different potential from those directed downward, leading to an asymmetry in the conductance with respect to reversal of B. A similar phenomenon occurs for $\langle g_1^{\mathrm{even}}\rangle$, where the billiard asymmetric with respect to reversal of V, device B, has the largest asymmetric contribution to the part of the nonlinear conductance associated with a reversal of bias.

The role of device asymmetry becomes more apparent when the nonlinear terms $\langle g_1^{\mathrm{even}}\rangle V$ and $\langle g_1^{\mathrm{odd}}\rangle BV$ are plotted with V and B for all billiards in Fig. 3. Significant rectification effects are seen for device B with increasing bias [see Figs. 3(c) and 3(a)], while the asymmetric terms for devices C and D grow significantly with B and are maximized for the combined effect of large B and V [Fig. 3(b)]. At high B and V, significant symmetry breaking is seen for all devices which contain intentional asymmetry and the magnitude of $\langle g_1^{\mathrm{odd}}\rangle BV$ approaches the order of magnitude of the fluctuations. For example, the $\langle g_1^{\mathrm{odd}}\rangle BV$ term for device C is half the size of the fluctuations ($0.04e^2/h$) at $B = 0.5$ T and $V = 1$ mV. Importantly, note that we observe different values of $\langle g_1^{\mathrm{odd}}\rangle$ depending on the billiard, suggesting that conductor geometry plays a role in nonlinear effects. For instance, device C has a larger asymmetric contribution to the nonlinear conductance than device D. A likely cause of this could be decoherence effects: In linear response the rms of the fluctuations for D is less than half that for C, which may be due to the difference in size. Smaller fluctuations would lead to overall smaller observed asymmetries due to nonlinear contributions.

To further investigate the breakdown of conductance symmetry, we extend our study to the statistical qualities of the asymmetric nonlinear MCF by investigating the spectral density of the fluctuations. For all the billiards presented here, the power spectra of the MCF display $1/f^{\alpha}$ scaling, where $f = 1/\Delta B$ is the magnetic frequency and α is the spectral exponent of the power law scaling relationship and characterizes the entire spectral content of the fluctuations [12]. In Fig. 4 we show that α increases with V. A similar increase in α is seen with temperature for MCF measured at $V = 0$ and the dependence of α on V is consistent with an increase in overall electron temperature due to the applied bias [13]. Unexpectedly, however, α evolves asymmetrically with B and V for devices C and D [Figs. 4(c) and 4(d)], indicating that the entire spectral density of the MCF evolves with B and V in an asymmetric manner. This translation of the device asymmetry to such a holistic quality of the MCF is intriguing. Strikingly, we find that α is asymmetric in B and V only for the UD

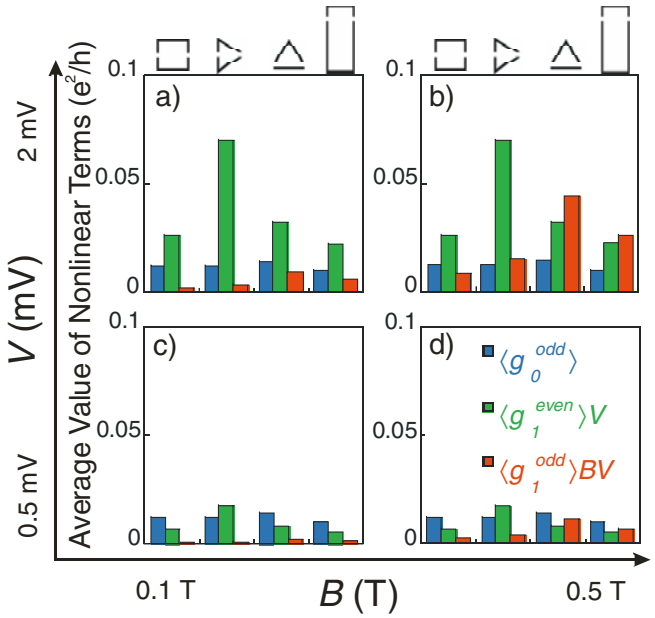

FIG. 3 (color online). The nonlinear terms $\langle g_0^{\mathrm{odd}}\rangle$, $\langle g_1^{\mathrm{even}}\rangle V$, and $\langle g_1^{\mathrm{odd}}\rangle BV$ for each of the devices (indicated by the illustrations above the plots) for both low and high V and B.

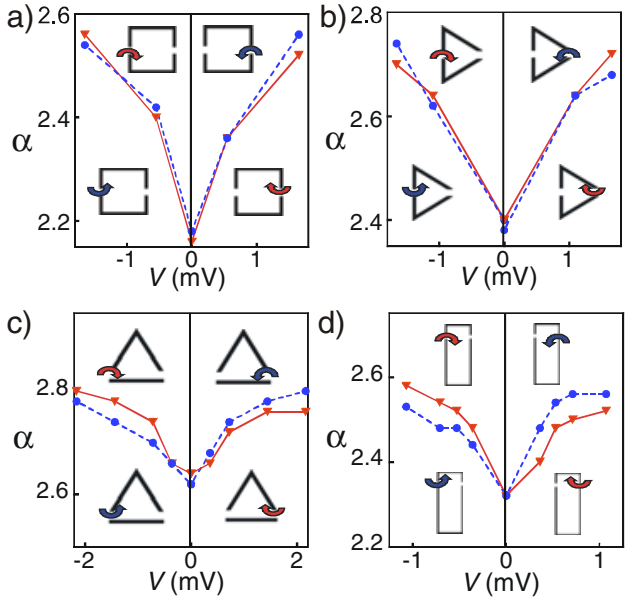

FIG. 4 (color online). (a), (b), (c), (d) The spectral exponent α of the MCF power spectrum as a function of $\pm V$ for $\pm B$ for devices A, B, C, D, respectively. The circles and triangles are taken at $+B$ and $-B$ respectively. Curves are provided as a guide to the eye. Illustrations indicate the injection conditions for each of the four cases, where $+V$ is directed to the left and $+B$ is into the page.

asymmetric billiards [Figs. 4(c) and 4(d)], but not for the LR asymmetric billiards [Figs. 4(a) and 4(b)]. One way of interpreting this observation is to consider the geometry of electron injection into the billiard, depending on the direction of B and V ($+B$ defined into the page and $+V$ to the left), as illustrated by the arrows in Fig. 4. For example, in the UD asymmetric device D MCF associated with electrons that initially enter the upper half of the billiard consistently show a smaller α value than MCF associated with electrons that enter the lower half [notice the reversal of the solid and dashed lines at zero bias in Fig. 4(d)]. In contrast, for device B, where the upper and lower half and the billiard are nominally the same, no such asymmetry in B is observed [see Fig. 4(b)]. In other words, the symmetry, or lack thereof, inherent in the billiard geometry with respect to a reversal of B translates into symmetry, or lack thereof, in the spectral content of the fluctuations. This effect is not captured by the BV term in the nonlinear conductance, and we are unaware of any theory which predicts this behavior.

The analysis used here is based on simple symmetry arguments and is thus general and can be used in both the classical and quantum regimes. In order to characterize the asymmetric contribution to the nonlinear conductance up to the high field ($B \gg B_c$) and high voltage ($V \gg E_s/e$) regime, we averaged the fluctuations (arising from quantum interference effects) in the measured asymmetry with B over many correlation fields. In contrast, the recent theories [6,7] predict the coefficient associated with the nonlinear term proportional to BV for $V < E_s/e$ and $B < B_c$. In order to determine if these distinct quantities are signatures of the same underlying physical processes, a more comprehensive theory is needed which extends to higher B and V.

We thank M. Büttiker and D. Sánchez for useful discussion and W. Seifert for providing the 2DEG material. Financially supported by the NSF IGERT Program (C. A. M.), NSF CAREER Program, (H. L.), and a Cottrell stipend (R. P. T.).

Note added.—Recently, we became aware of related experimental work in carbon nanotubes [14] and quantum dots in the $B < B_c$ field range [15].

*Corresponding author.
Email address: cmar@monkeyjump.org
†Email address: linke@uoregon.edu

[1] L. Onsager, Phys. Rev. **38**, 2265 (1931); H. B. G. Casimir, Rev. Mod. Phys. **17**, 343 (1945).
[2] M. Büttiker, Phys. Rev. Lett. **57**, 1761 (1986).
[3] B. L. Al'tshuler and D. E. Khmel'nitskii, JETP Lett. **42**, 359 (1985); T. Christen and M. Büttiker, Europhys. Lett. **35**, 523 (1996); R. A. Webb *et al.*, Phys. Rev. B **37**, 8455 (1988); H. Linke *et al.*, Europhys. Lett. **44**, 341 (1998).
[4] A. Löfgren *et al.*, Phys. Rev. Lett. **92**, 046803 (2004).
[5] A. Löfgren *et al.* (to be published).
[6] B. Spivak and A. Zyuzin, Phys. Rev. Lett. **93**, 226801 (2004).
[7] D. Sánchez and M. Büttiker, Phys. Rev. Lett. **93**, 106802 (2004).
[8] This sum isolates the first order term in the expansion by eliminating the next highest term in V, as opposed to just taking one of the sums $g(+B, +V) - g(-B, +V)$ or $g(+B, -V) - g(-B, -V)$.
[9] T. P. Martin *et al.*, Superlattices Microstruct. **34**, 179 (2003).
[10] J. P. Bird *et al.*, Surf. Sci. **361–362**, 730 (1996).
[11] C. W. J. Beenakker and H. van Houten, in *Solid State Physics*, edited by H. Ehrenreich and D. Turnbull (Academic Press, Boston, 1991), Vol. 44.
[12] $1/f^{\alpha}$ scaling is a signature of fractal behavior, see, for example, J.-F. Gouyet, *Physics and Fractal Structures* (Springer-Verlag, New York, 1996); The fractal behavior of the MCF observed in these devices is consistent with previously observed fractal conductance fluctuations in similar systems [9,16].
[13] H. Linke *et al.*, Phys. Status Solidi B **204**, 318 (1997); M. Switkes *et al.*, Appl. Phys. Lett. **72**, 471 (1998); A. G. Huibers *et al.*, Phys. Rev. Lett. **83**, 5090 (1999); C. A. Marlow *et al.*, cond-mat/0512132.
[14] J. Wei *et al.*, cond-mat/0506275.
[15] D. M. Zumbuhl *et al.*, cond-mat/0508766.
[16] C. A. Marlow *et al.* (to be published).